Coupled plasmon wave dynamics beyond anomalous reflection: phase gradient Copper metasurface for visible to the near infrared spectrum.

1.1 TRAPEZOID LENGTH PARAMETER.

To check the Anomalous reflection performance, we have chosen the four incremental lengths of the trapezoids. Suppose we plot the area coverage from the anomalous reflection (AR) efficiency curve for broadband and plot it against trapezoid length. In that case, we can see the trend of total broadband AR reflection efficiency per nm of trapezoid length increment.

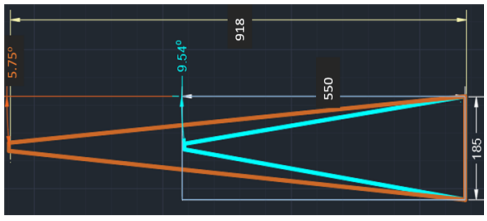

Table 1: Trapezoid dimension in (nm)

Length	Base	Px	Py
918	185	980	349
825	185	887	349
700	185	762	349
550	185	612	349

(a)

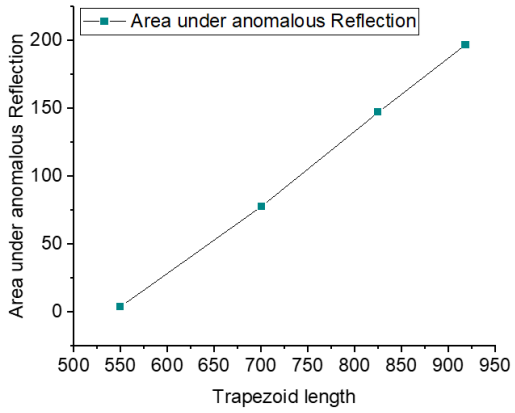

(b)

Figure S1.1. (a) Shape comparison between the 550L trapezoid and 918L trapezoid. (b) Different length trapezoid's total broadband reflection efficiency for anomalous beam steering.

1.2. Reflection efficiency for four different lengths of trapezoid at specular and (±1,0) order and far-field beam steering.

Far-field from simulated wavelength dependent, angle-resolved reflection orders for all four length-trapezoid for both TE and TM normal incident indicating the magnitude of (-1,0) order remains almost constant but (1,0) increases rapidly with trapezoid's length increment.

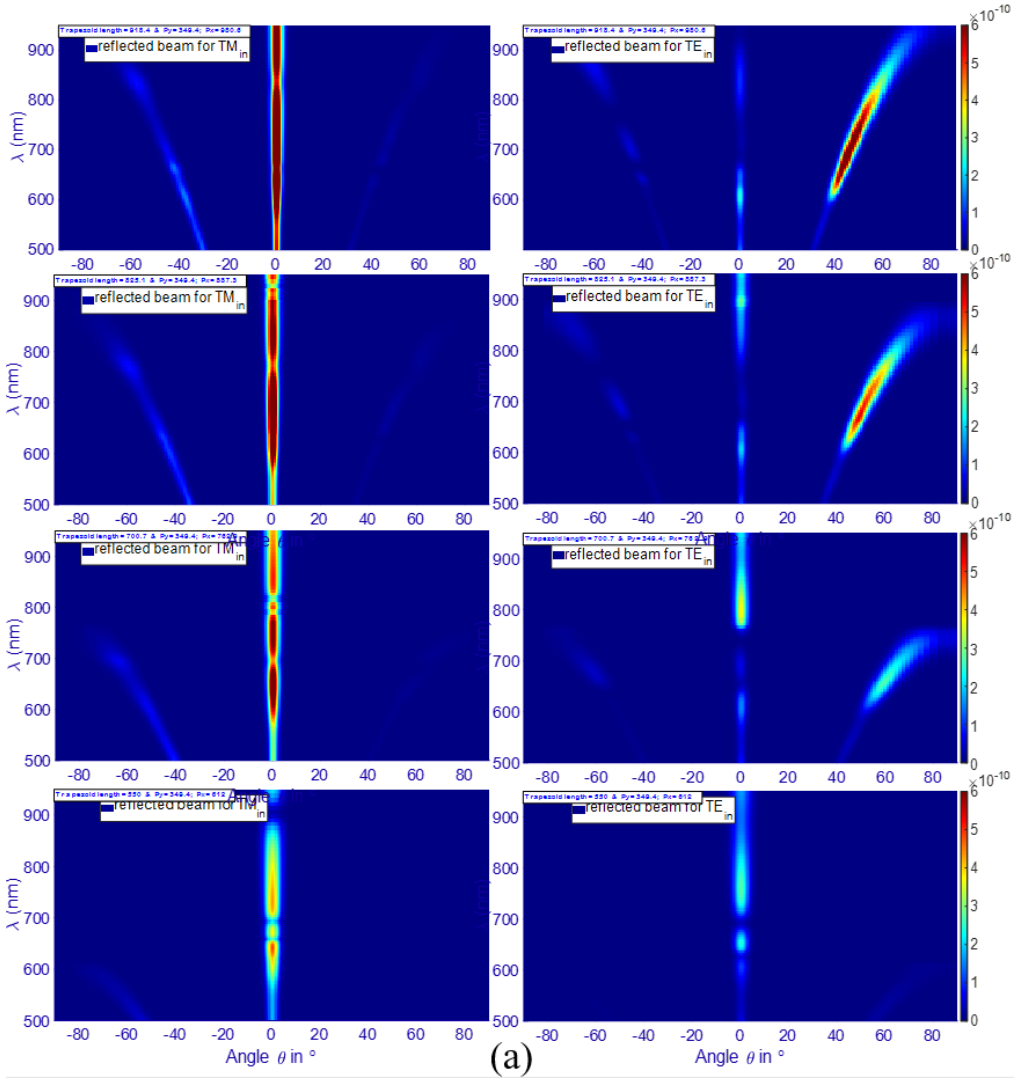
reflected beam for TM in
reflected beam for TE in
λ (nm)
Angle θ in °
×10^-10

(a)

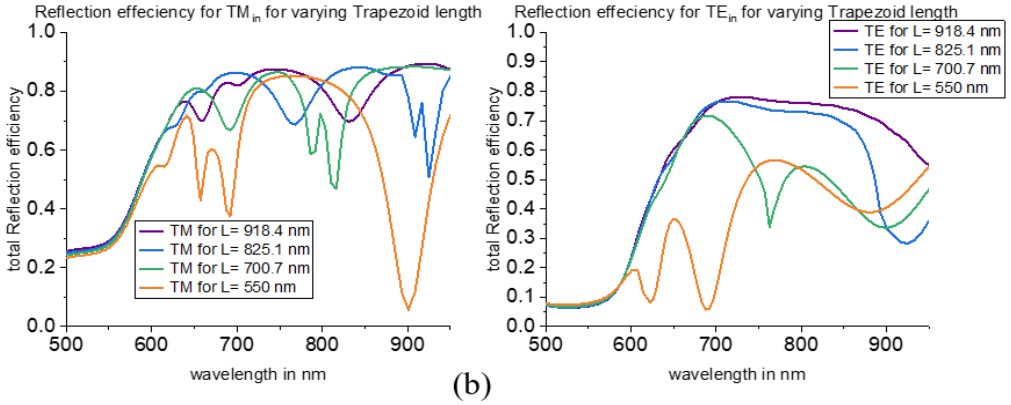
Reflection effeciency for TM in for varying Trapezoid length
Reflection effeciency for TE in for varying Trapezoid length
total Reflection efficiency
wavelength in nm
TM for L= 918.4 nm
TM for L= 825.1 nm
TM for L= 700.7 nm
TM for L= 550 nm
TE for L= 918.4 nm
TE for L= 825.1 nm
TE for L= 700.7 nm
TE for L= 550 nm

(b)

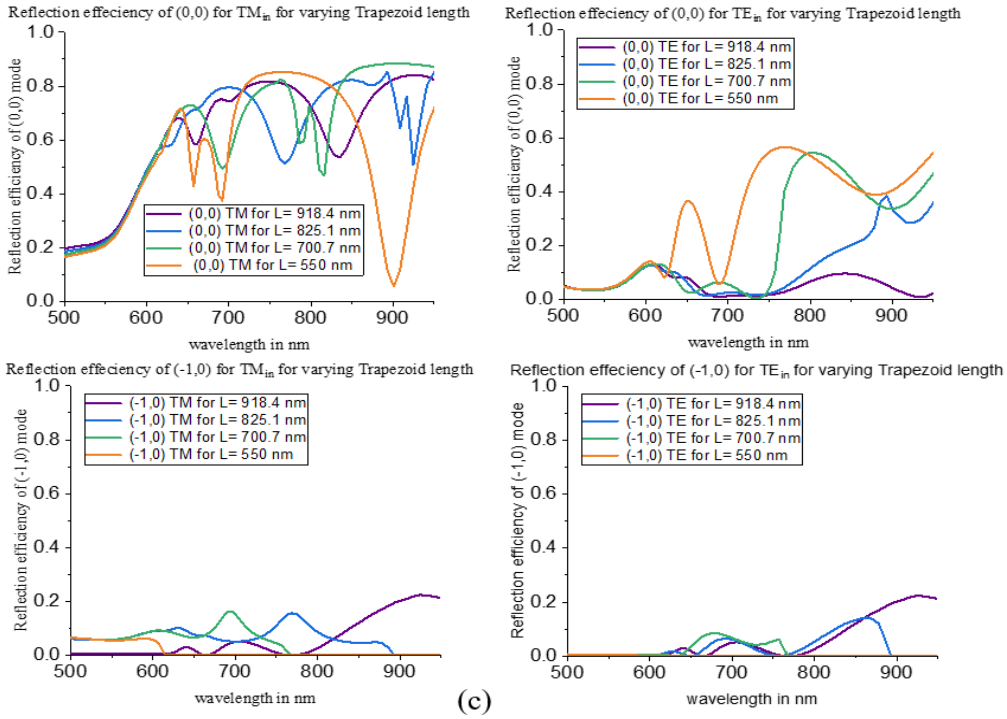

Figure S1.2**.** Figure S1.2: (a) Different length trapezoid wavelength dependent reflection orders at far-field and their angler projection. Top to bottom from 918L to 550L sequentially. The left side for TM incidence and the right side for TE incidence. (b) Different length trapezoid wavelength dependent total reflection efficiencies. (c) Different length trapezoid wavelength dependent reflection efficiencies by different orders. Top for Specular or (0,0) order, bottom (0,-1) order. The left side for TM incidence and the right side for TE incidence. The (0,1) order or the Anomalous reflection has been shown on main text figure 1d for TE incidence. The reflection efficiency for TM incidence of that order is almost negligible, so not presented here.

2.1. Dispersion curve for SiO_2/Cu and Air/Cu interface

To understand the SPP modes at the metal-dielectric interface assuming a semi-infinite XY plane of the metal-dielectric-metal layer. For normal incident incidence TM wave with **E** = (E_x, 0, E_z) and so, **H**= (0, H_y, 0) in a metal-dielectric-metal (MIM) waveguide type structure the solution for modes [1–4] :

$$\tanh\left(\frac{k_d h}{2}\right) = -\begin{cases}\frac{\varepsilon_d k_m}{\varepsilon_m k_d} & \text{symmetric} \\ \frac{\varepsilon_m k_d}{\varepsilon_d k_m} & \text{antisymmetric}\end{cases} \tag{S1}$$

This is the equation of the guided mode, with

$$k_m = \sqrt{k_x^2 - \varepsilon_m k} \tag{S2}$$

$$k_d = \sqrt{k_x^2 - \varepsilon_d k} \tag{S3}$$

Here, κ_m and κ_d are the **z** component inside the metal and the dielectric layer, respectively,

called transverse wave vectors. h is the width of the dielectric layer; K is the free space wave vector and κ_x in the propagation constant of the traveling wave at the interface. With the boundary condition of the continuity $E_{xd} = E_{xm}$ and $H_{yd} = H_{ym}$ components and the relation between the normal components, κ_m and κ_d and dielectric constants of the metal and dielectric media becomes:

$$\frac{k_m}{k_d} = -\frac{\varepsilon_m}{\varepsilon_d} \tag{S4}$$

So, from the equations (S1) and (S4), solving for the component of the wave vector in the direction of propagation, we get the SPP dispersion relation:

$$k_{SPP} = k\sqrt{\frac{\varepsilon_d\,\varepsilon_m}{\varepsilon_d+\varepsilon_m}} \tag{S5}$$

$$k_{SPP} = k'_{SPP} + ik''_{SPP} \tag{S6}$$

Here, the prime means the real part, and the double prime means the imaginary parts.

Figure S2.1a compares SiO_2/Cu dispersion with air/Cu dispersion from the same interface layer but moving the dipole source to the backplane for Cu/air interface; for the SiO_2 thickness 50 nm and Cu 100 nm. The color bar indicates the coupling strength. To excite SPP with the incident free space photon, the momentum and wave vector must match to couple light to the SPP mode at the interface when the dielectric constant match, ε_m=-ε_d. There are many techniques and configurations of these SPP couplers, mainly prison coupler, grating coupler, fiber, and waveguide coupler [5–8]. We can see here, beyond the phase-matching region at the low-frequency light can be coupled to the plasmonic modes at 303 THz (990 nm of λ_0) at Cu/SiO_2 interface and at 470 THz (637 nm of λ_0) at Cu/air interface.

Long-range SPP propagation is crucial in photonics circuits and plasmonic devices in optical communication sub-system design [8–10]. At the visible to infrared, the SPP propagation range is low because of loss in metal. The length of SPP propagation is defined as the distance where the intensity of any mode that decays to a factor of 1/e from its origination point called δ_{spp}. Theoretically, we can calculate it from the imaginary part of the SPP wavevector as that takes care of the ohmic losses in metal [9,11–14]. From equation (S6)

$$\delta_{SPP} = \frac{1}{2\,k''_{SPP}} = \frac{\lambda}{2\pi}\left(\frac{\varepsilon'^{\,2}_m}{\varepsilon''_m}\right)\left(\frac{\varepsilon'_d+\varepsilon'_m}{\varepsilon'_m\,\varepsilon'_d}\right)^{3/2} \tag{S7}$$

Figures S2.1 b and c show theoretically calculated SPP propagation length and the propagation vectors, respectively. The data was taken from palik [15].

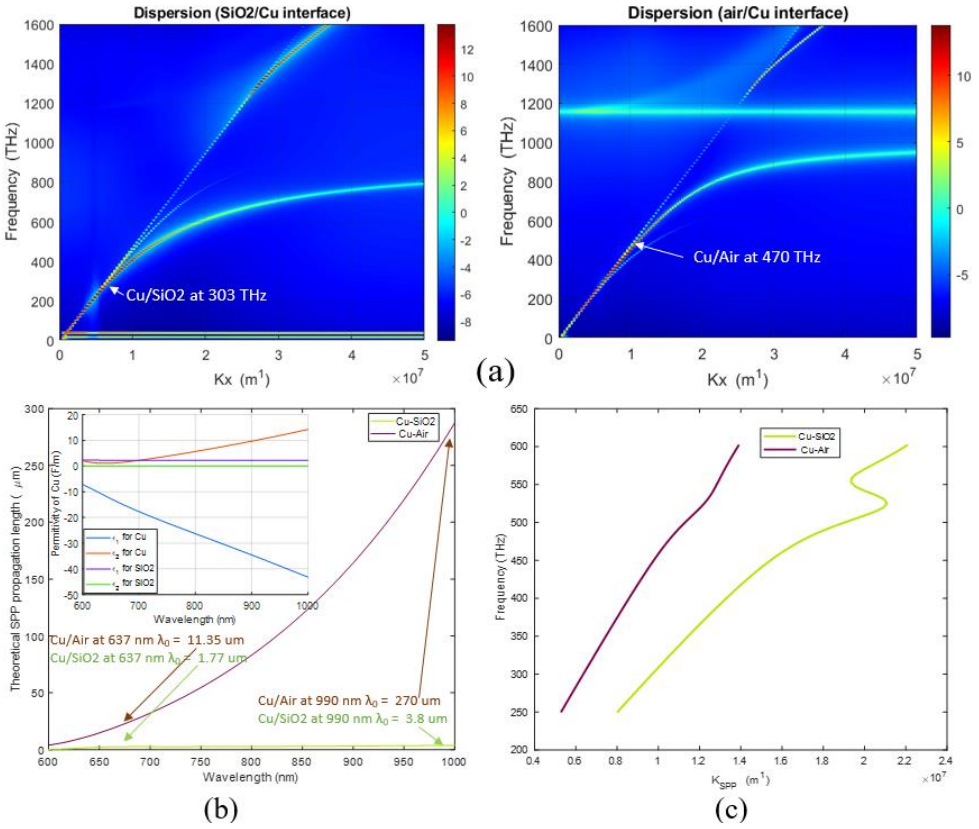

Figure S2.1. (a) Dispersion for SiO_2/Cu layer interface (left side) and dispersion for air/Cu layer interface (right side). (b) Theoretical SPP propagation length vs. incidence wavelength. The inset shows the real and the imaginary part of the permittivity Cu and SiO_2. Theoretically calculated (c) K_{SPP} as mentioned in equation S6.

2.2. SPP coupling difference between Rectangle and Trapezoid under broadband illumination of the plane wave source.

GSP resonance modes exist between the gap of nanoantenna's and the spacer layer; their resonance overlap can create supermodes [16]. The mode profile evolves differently at the tip and base sides as the tip is 20 nm wide, expected to have Localized Surface Plasmon (LSP) behavior while the base side retains bulk plasmon behavior. The resonance excitation enhances the field amplitude almost twice (figure 4c of main text). Comparing the E_z field excitation in the gap between tip to base (trapezoid) and base to base (rectangle) in figure S2.2 and the visualization 1, visualization 2 files, we see the induced field from tip to another base set the unidirectional propagating plasmonic oscillation. Here we reported two specific wavelength phenomena for mode coupling, 637 nm of λ for 550L trapezoid and rectangle and 990 nm of λ for 918L trapezoid and rectangle where the coupled SPP mode of these two-length types of nanoantenna is supported by the SiO_2/Cu layer; so propagating SPP mode can be guided out. Here we particularly focused on the E field arrow as it indicates the behavior of SPSPP for 550L and LRSPP for 918L trapezoid between top nanoantenna and bottom Cu layer as a whole system that was found in the corrugated thin metal film [17].

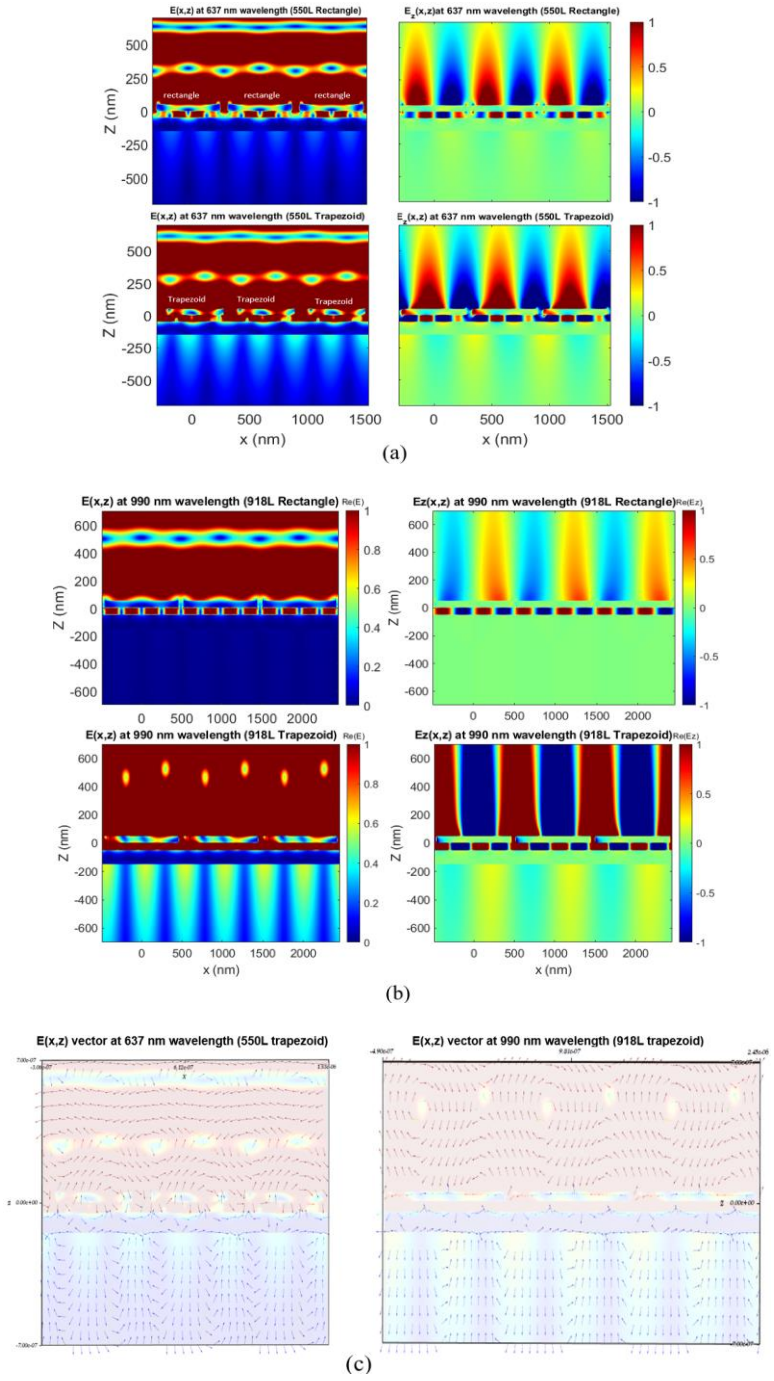

Figure S2.2. (a) Simulated total E-field and Ez field in XZ plane at Y=0. (cross-section for three trapezoids in a row, alone middle line through the Trapezoids tip to base. The left side is the tip direction, and the right side is the base direction aligned one after another towards the x-direction, occupying from z = 0 to 50 nm. The continuous SiO2 layer occupies Z= -50 to 0 nm, and the Cu bottom is from z = -150 to -50 nm. The plane wave TM normal incidence source is at 750 nm top and injected towards backward Z direction. (a) top row for 550L rectangle and the bottom row for 550L trapezoid at 637 nm of wavelength. (b) top row for 918L rectangle and the bottom row for 918L trapezoid at 990 nm of wavelength. (c) Vector field profile for both 550L and 918L trapezoids at the corresponding wavelength.

2.3. Simulated wavelength dependent Ez(λ,z) and E(λ,z) profile at a particular x-position:

To look at the effect from the different regions of nanoantenna structures that can excite the plasmon modes differently, we compare this series of Ez(λ,z) and E(λ,z) field profiles. In terms of field excitation compared to the rectangle, the trapezoid tip and base side are different, as well as the middle position. This is another way to check which length of the trapezoid will be able to couple light at which wavelength efficiently. For both cases, the x-position for the tip and base are chosen about 25 nm inside the nanoantenna structure to avoid edge effect from finite meshing error. The FDTD simulation was done with the 13th mesh order. The wavelength-dependent Ez profile also indicates the field penetration is more on the tip side (x=-252 nm, -434 nm) through the SiO_2 layer at the lower wavelength.

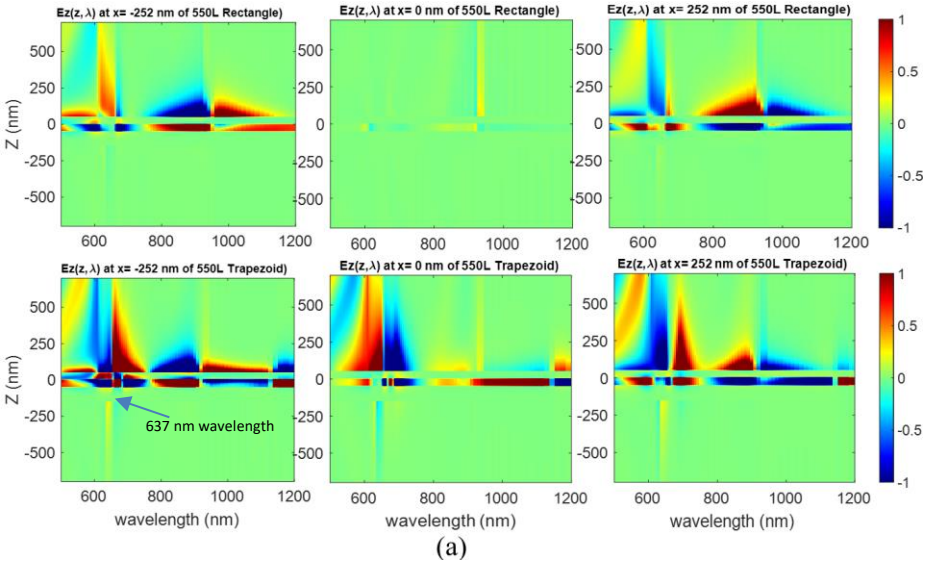

(a)

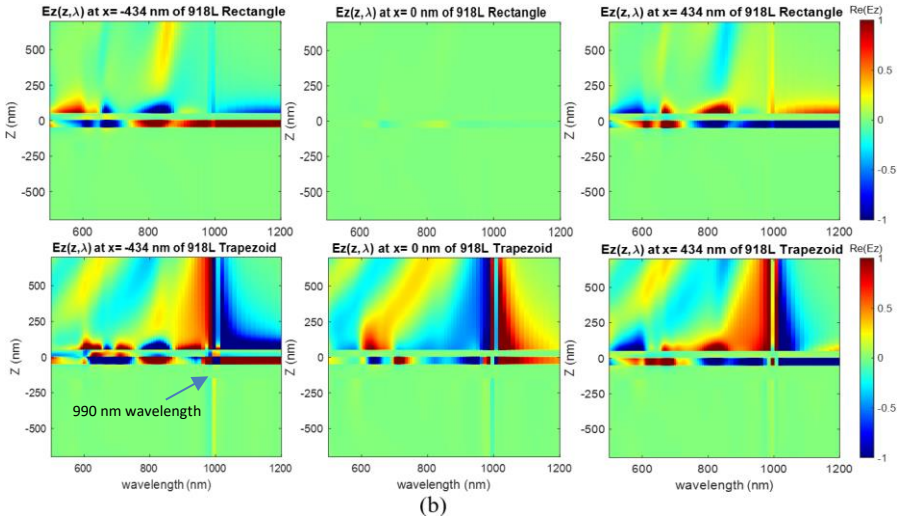

(b)

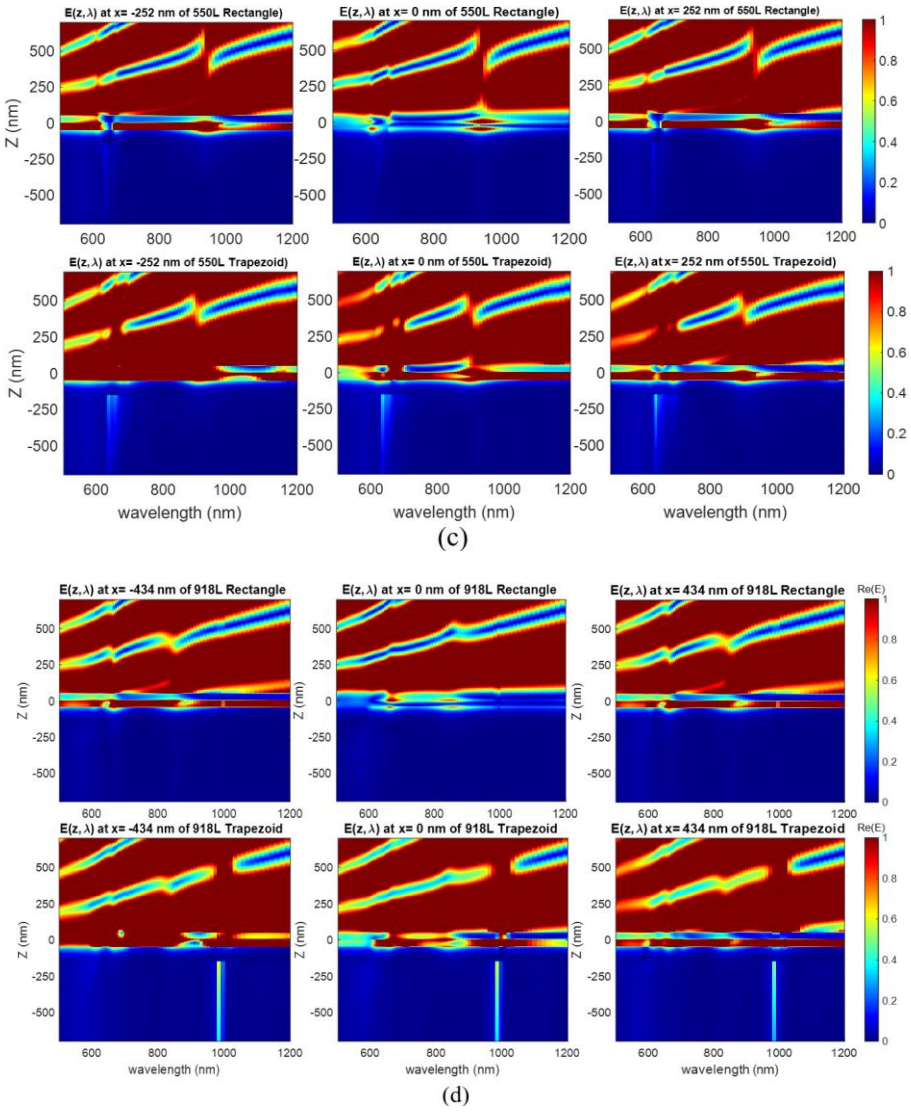

Figure S2.3. Simulated wavelength dependent Ez-field component in particular x positions for the cross-section in YZ plane. The simulation has been done in the same configuration as figure S2.2. Among all these images, the left side one is at the tip position of the first rectangle or trapezoid at x= -252, 0, 252 nm (just at 25 nm inside from the tip of the trapezoid or for the edge of the rectangle and at the middle). (a) The top row 550L rectangle and the bottom row 550L trapezoid (b) are the same for the 918L rectangle and trapezoid at x= -434, 0, 434 nm. (c) E field for 550L rectangle top row and trapezoid bottom row. (d) same for the 918L rectangle and trapezoid.

3. Simulated E(x,z) and Ez(x,z) profile of long-range SPP wave varying the Cu-bottom layer thickness.

For the long-range propagation behavior of the couple SPP wave, the simulation has been done with an extended FDTD region in the x-direction (figure 6 in main text), beyond the trapezoid or rectangle area. Only the trapezoids and rectangles area has been illuminated by the TFSF source from the top with all PML boundaries. The net power propagation shows the prominently unidirectional flow from the trapezoid region. With the E and Ez field component

profile, we can verify that the SPP wave guided out as a coupled linearly polarized pattern. Once the field is excited under the Cu-trapezoid/SiO_2 layer, the transverse nature of coupled plasmon between the top Cu/SiO_2 and bottom Cu/air interfaces survive long (~10 μm) as shown in the movie (visualization 3 to visualization 8). We increase the thickness of the Cu bottom layer to 200 and 500 to see the long-range coupling strength. The Symmetric (for 550L) and antisymmetric (for 918L) modes remain the same with metal layer thickness increment. Yet, there is a noticeable difference in oscillatory pattern and power flow compared with main text figure 6e and 6f. The presence of the LRSPP can also verify alone with figure S2.2c, so the device idea with 918L trapezoid comes with less constraint on the bottom layer thickness.

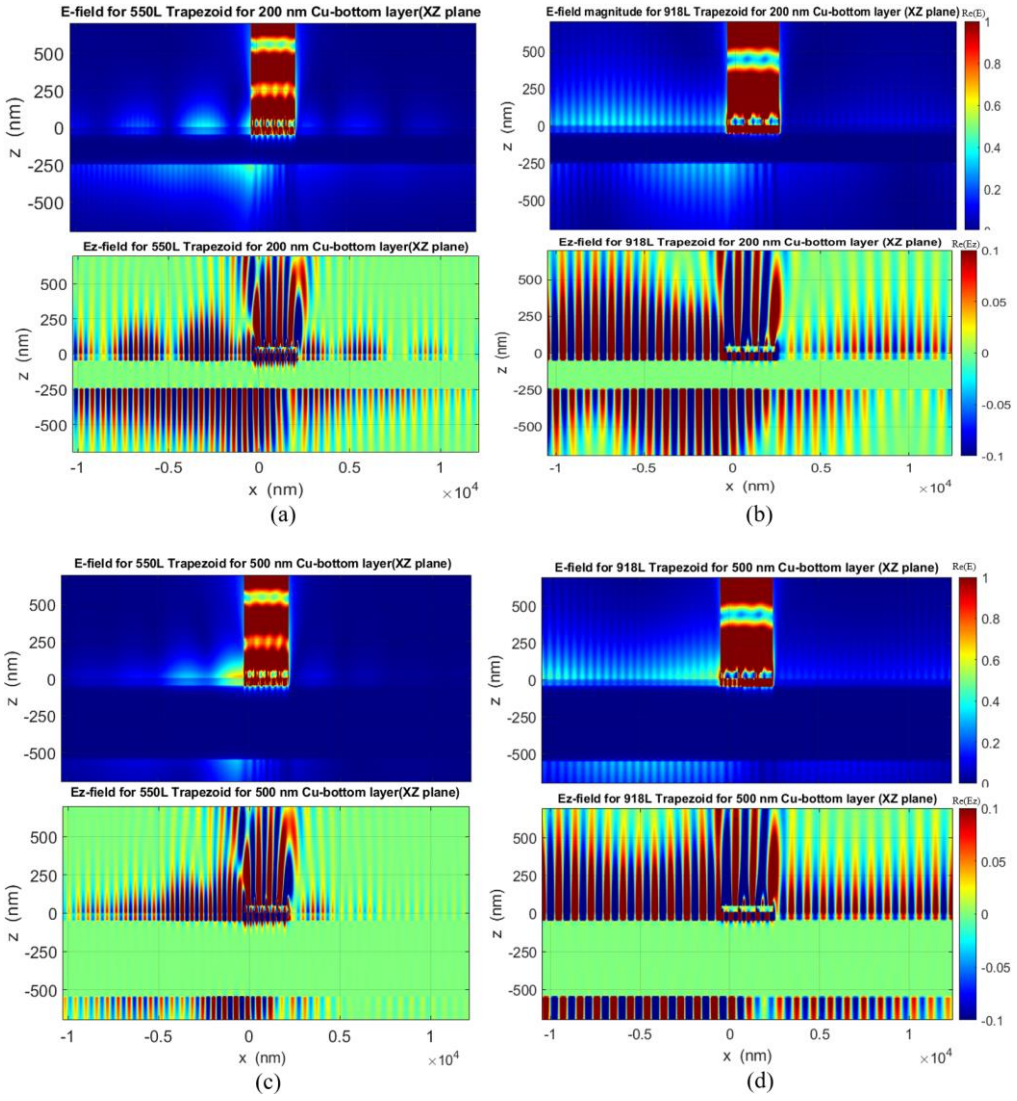

Figure S3. SPP coupling with Cu-bottom layer thickness variation. Simulated total E-field and Ez field in XZ plane at Y=0, the same configuration as main text figure 7. (a) For 200 nm Cu-bottom layer of 550L trapezoid at 637 nm of wavelength. (b) For 200 nm Cu-bottom layer of 918L trapezoid at 990 nm of wavelength. (c) For 500 nm Cu-bottom layer of 550L trapezoid at 637 nm of wavelength (d) For 500 nm Cu-bottom layer of 918L trapezoid at 990 nm of wavelength.

Bibliography:

1. B. Prade, J. Y. Vinet, and A. Mysyrowicz, "Guided optical waves in planar heterostructures with negative dielectric constant," Physical Review B **44**(24), 13556–13572 (1991).

2. "Chapter 1 Optical Properties of Plasmonic Materials," in (2017).

3. A. Pors and S. I. Bozhevolnyi, "Plasmonic metasurfaces for efficient phase control in reflection," Optics Express **21**(22), 27438 (2013).

4. A. Davoyan, "Backward and forward modes guided by metal-dielectric-metal plasmonic waveguides," Journal of Nanophotonics **4**(1), 043509 (2010).

5. A. v. Zayats and I. I. Smolyaninov, "Near-field photonics: Surface plasmon polaritons and localized surface plasmons," Journal of Optics A: Pure and Applied Optics **5**(4), (2003).

6. Z. Han and E. Forsberg, "Surface plasmon bragg gratings formed in metal-insulator-metal waveguides," IEEE Photonics Technology Letters **19**(2), 91–93 (2007).

7. J. Guo and H. Leong, "Mode splitting of surface plasmon resonance in super-period metal nanohole array gratings," Applied Physics Letters **101**(24), (2012).

8. J. Zhang, L. Zhang, and W. Xu, "Surface plasmon polaritons: Physics and applications," Journal of Physics D: Applied Physics **45**(11), (2012).

9. P. Berini, "Long-range surface plasmon polaritons," Advances in Optics and Photonics **1**(3), 484 (2009).

10. M. I. Stockman, "Nanoplasmonics: past, present, and glimpse into future," Optics Express **19**(22), 22029–22106 (2011).

11. J. Li, J. Li, H. Zhou, G. Zhang, H. Liu, S. Wang, and F. Yi, "Plasmonic metamaterial absorbers with strong coupling effects for small pixel infrared detectors," Optics Express **29**(15), 22907 (2021).

12. J. Zhang, L. Zhang, and W. Xu, "Surface plasmon polaritons: Physics and applications," Journal of Physics D: Applied Physics **45**(11), (2012).

13. M. N. Gadalla, K. Chaudhary, C. M. Zgrabik, F. Capasso, and E. L. Hu, "Imaging of surface plasmon polaritons in low-loss highly metallic titanium nitride thin films in visible and infrared regimes," Optics Express **28**(10), 14536 (2020).

14. Y. Dai, *Imaging Light with Photoelectrons on the Nano-Femto Scale* (2020).

15. edited by E. D. Palik, *Handbook of Optical Constants of Solids* (Orlando : Academic Press, 1985., 1985).

16. P. Qiao, W. Yang, and C. J. Chang-hasnain, "Recent advances in high-contrast metastructures , metasurfaces and photonic crystals," 1–58 (n.d.).

17. Z. Chen, I. R. Hooper, and J. R. Sambles, "Coupled surface plasmons on thin silver gratings," Journal of Optics A: Pure and Applied Optics **10**(1), 1–9 (2008).